Structural and Optical Properties of $Ge_{20}Se_{70}Zn_{10}$ Thin Films

A. Elwhab B. Alwany[1], Mohammed A. Algradee[2], M. M. Hafith[3], M. A. Abdel-Rahim[4]

[1,2]Physics Department Faculty of Science, Ibb University, Ibb, Yemen

[3,4]Physics Department Faculty of Science, Assuit University, Assuit, Egypt

([1]abdualwhab@yahoo.com)

Abstract- Thin films having composition $Ge_{20}Se_{70}Zn_{10}$ were deposited onto glass substrates by the vacuum thermal evaporation technique. Effective crystallite size and strain are determined by the method of variance analysis of the X-ray diffraction line profiles for the films. Reflectance and transmittance at normal incidence of the as-deposited and annealed samples are measured by spectrophotometer in the spectral range of $300 - 2500$ nm. Direct optical band gap (E_g) and Urbach energy (E_U) are calculated from the absorption coefficient. Analytical relations are used to deduce the real and imaginary refractive indices at each scanned wavelength from the measured reflectance and transmittance. Dispersive parameters of Wemple-DiDomenico dispersion's relations are also deduced.

Keywords- Thin Films, Optical Properties, Dispersive Parameters

I. INTRODUCTION

Chalcogenide glasses have received much attention for their applications in optical data storage, integrated optics, optical imaging and infrared optics [1–3]. These applications were attributed to their transparency in the infrared (IR) region, low phonon energies and easy to fabricate [4–6]. The Zn–Se binary glass has gained much attention due to a wide-band-gap II–VI semiconductor with a gap of 2.8 eV [7–13]. The effect of Zn content in Zn–Se binary glass on the optical properties has been investigated in our previous work [9, 10]. The optical properties of Ge–Se chalcogenide glasses have been extensively studied. Adding indium to Ge-Se glass is considered as an effective way controlling their optical properties. Also, these glasses (Ge-Se-In) have great of interest because their ability to create glasses with a wide area of compositions [14]. In addition, the optical energy gap of Ge-Se-Te has been investigated for as-prepared and annealed films as a function of incident wavelength (photon energy) [15]. In this study, the optical energy gap increases with increasing annealing temperature. Chen et al. [16] investigated the optical properties of the Ge–Se–Te chalcogenide glasses to find the relation between optical band gaps and the glass constituents. The optical band gaps were found to be in the range of 0.19–0.32 eV [17]. Many studies were carried out concerning thin films of Ge–Se [18] and Se–Te [19–21] system to investigate the optical, electrical and structural properties. Also, chalcogenide glasses containing Sb [22] and Ge [23–25] were

studied. On the other hand, the chalcogenide semiconductors of Se-Te are investigated by various studies because the glass forming of this system expands to whole substitution of Se by Te and their applicability as solid state devices [26–29]. The addition of Germanium element of this Se-Te system leads to increase the glass transition temperature and improve the thermal stability and the optical properties of the ternary glass [30–33].

Crystallization of present ternary chalcogenide glasses is accompanied by a change their properties. Separation of different crystalline phases with heat treatment has been observed in our glasses. The effect of heat treatment is discussed on the basis of amorphous crystalline transformation [34–36].

Optical spectra are used to determine the band structure and the energy gap of chalcogenide glasses, because the analysis of the optical spectra is one of the most productive tools for studying the energy diagram of both amorphous and crystalline materials. The degree of disorder and defects in the amorphous structure changes due to annealing temperature [37]. To our knowledge, not enough optical investigations have been made of Ge–Zn–Se thin films.

Thin films have been prepared by various techniques such as thermal evaporation under vacuum, solution growth spray pyrolysis, molecular beam epitaxy (MBE) organo-metallic chemical vapor deposition, etc. but the used method (thermal evaporation) was available and very common due to low cost, simplicity and scalability deposit onto large area substrates. Moreover the films produced with this method are highly adherent and uniform [9, 10].

The aim of the present work is to determine the effect of Ge additives and heat treatment on the structural (by X-ray diffraction) and optical properties of Ge–Zn–Se thin films by analysis of the transmittance T and reflectance R spectra of these films.

II. EXPERIMENTAL DETAILS

A. Bulk samples preparation

Bulk $Ge_{20}Se_{70}Zn_{10}$ was prepared by the melt-quench technique. Appropriate amounts of high purity (99.999%) Ge, Zn and Se (from Aldrich, UK) were weighted (5 g total weight) according to their atomic percentage. The weighted elements

were placed into a quartz glass ampoule and sealed under vacuum of 10^{-4} Torr. The sealed ampoule was heated in Heraus programmable tube furnace (type R 07115), the heating rate was approximately 3.5 K/min. The temperature was kept at 1173 K for 24 h. The ampoule was manually stirred for realizing the homogeneity of the composition. After that, the ampoule was quenched into ice-cooled water.

B. Thin films preparation

Thin films of $Ge_{20}Se_{70}Zn_{10}$ were prepared by thermal evaporation at vacuum of 10^{-5} Torr from the bulk of $Ge_{20}Se_{70}Zn_{10}$ using Edward 306E system. A constant evaporation rate (3 nm/sec) was used to deposit the films. The evaporation rates as well as the films thickness were controlled using a quartz crystal monitor (FTM5), where the films thickness were (300 nm). $Ge_{20}Se_{70}Zn_{10}$ films were annealed at different temperature ($373 \leq T_{ann} \leq 423$ K) for one hour under gas Nitrogen.

C. X-ray diffraction apparatus setup

The amorphous and crystalline phases for as-deposited and annealed films were examined by X-ray diffraction analysis at room temperature. The data are collected using Philips (type1710) diffractometer with CuK_{α} radiation. The spectra data were acquired within the range of $2\theta = 4^{0} - 90^{0}$ at a scanning step and speed of 0.02 and 0.06 %, respectively. The radiation source was CuK_{α} with a graphite monochromator where $\lambda= 1.54178$ Å at 49 kV and 30 mA. The divergence and receiving slits were fixed at 1^{0} and 0.2 mm, respectively.

D. Spectrophotometric measurements

In order to determine the absorption coefficient α and the optical constant of the films as a function of the incident light wavelength, a computer aided double beam spectrophotometer (Shimadzu 2101 UV–VIS) was used to record the reflectance, R, and transmittance, T, data for the prepared films at normal incidence of light. The measurements were carried out at room temperature, 23 °C, for the entire spectral range of wavelength from 300 to 2500 nm.

III. REFRACTIVE INDICES DETERMINATION

A. Analytical determination of complex refractive index

Refractive index is one of the fundamental properties for an optical material. Its real part is inversely proportional to the wave propagation velocity, while its imaginary part is related to the intensity attenuation inside the material. It is closely related to the electronic polarization of ions and the local field inside the material. The determination of the refractive indices of optical materials is crucial for applications in optical devices. The refractive index as a function of the wavelength is a critical design parameter for advanced photonic systems [38, 39].

In this work analytical expressions are used for the first time (to our knowledge) to retrieve the real and imaginary refractive indices taking into consideration incoherent multiple reflections inside the sample [40]. The relation between the measured transmittance, T, measured reflectance, R, and interface reflectance, R_{as}, is [40],

$$R_{as} = \frac{[2+T^2 -(1-R)^2]-\left\{[2+T^2 -(1-R)^2]^2 -4(2-R)R\right\}^{1/2}}{2(2-R)} \quad (1)$$

The imaginary part of the refractive index, k, is deduced as:

$$k = \frac{\lambda}{4\pi t} ln\left[\frac{TR_{as}}{(R-R_{as})}\right] \quad (2)$$

where t is the thickness of thin films,

The real part of the refractive index, n, is:

$$n = \frac{(1+R_{as})}{(1-R_{as})} + \left[\frac{4R_{as}}{(1-R_{as})^2} - k^2\right]^{1/2} \quad (3)$$

The absorption coefficient, α, of the glass materials are:

$$\alpha = \frac{4\pi k}{\lambda} \quad (4)$$

B. Real refractive index dispersion relation

The refractive index of a material is a complex quantity (real and imaginary), which describes not only the properties of material dispersion, but also its absorption. Wemple and DiDomenico (W–D) [41] described how to model real refractive index, n, data in a single oscillator model as a function of incident photon energy, E, as:

$$\frac{1}{n^2-1} = \frac{E_o}{E_d} - \frac{E^2}{E_0 E_d} \quad (5)$$

where E_o is the single oscillator energy related to an average band gap, and it corresponds to the distance between the centers of gravity of the valence and conduction bands, and E_d is the dispersion energy which measures the average strength of the interband optical transitions. In this relation, the dispersion was considered by electronic transitions. By plotting $(n^2 -1)^{-1}$ versus E^2 and fitting straight line E_o and E_d can be determined from the intercept and the slope.

The multiplication of oscillators concentration and oscillator strength per effective mass is written as:

$$Nf/m^* = \frac{4\pi^2 \varepsilon_o E_o E_d}{e^2 h^2} \quad (6)$$

where ε_o is the free space of dielectric constant (8.854×10^{-12} F/m), e is the charge of electronic and h is the Plank's constant. The refractive index at infinite wavelength, n_∞, considering only electronic transitions can be written as:

$$n_\infty = \sqrt{1 + \frac{E_d}{E_o}} \quad (7)$$

The lattice dielectric constant, (ε_L) and the ratio of the carrier concentration to the effective mass, (N/m^*) can be investigated by using the slope and intercept of the linear relation [10],

$$n^2 = \varepsilon_L - \left(\frac{e^2}{4\pi c^2 \varepsilon_0} \frac{N}{m^*}\right) \lambda^2 \quad (8)$$

where c, is the speed of light and λ, is the incident wavelength.

IV. OPTICAL BAND GAP AND URBACH ENERGY

The values of optical band gap (E_g) for as-deposited and annealed thin films were determined by analyzing the optical

data with the expression for the absorption coefficient, α. and the photon energy (E), [41] using the relation

$$\alpha E = A(E - E_g)^m \quad (9)$$

where the power m is a number which determines type of the optical transition (m = 1/2 for allowed direct transitions and, m = 2 for allowed indirect transitions), A is a constant which dependence on the electron transition probability and E_g is the optical band gap. The value of E_g is calculated by extrapolating the straight line portion of $(\alpha E)^2$ versus E for the direct optical band gap.

In the low absorption regions where the absorption coefficient laying between 10^2 and 10^4 cm^{-1}, are defined as Urbach's exponential tails region [42]. It is given by:

$$\alpha = \alpha_o e^{E/E_U} \quad (10)$$

where α_o is a constant and E_U is the Urbach energy interpreted as the width of the tails of localized states in the band gap. The equation (10) can be written as:

$$ln\alpha = ln\alpha_o + e^{E/E_U} \quad (11)$$

Plotting the dependence of ln(α) versus E should give a straight line. The inverse of the slope gives the band tail width (E_U) of the localized states at the band gap.

V. EXPERIMENTAL RESULTS AND DISCUSION

The morphology of the annealed $Ge_{20}Se_{70}Zn_{10}$ thin films was investigated using Scanning electron microscopy (SEM). The samples were gold coated before SEM examination to study the surface morphology. The scanning micrograph of the annealed $Ge_{20}Se_{70}Zn_{10}$ films are shown in Fig. 1(a, b). The microstructure for the annealed sample at 373 K for 1 h is shown in Fig. 1(a), it is clear that the crystalline phases are embedded in the amorphous matrix. In general, further increase of annealing temperature (annealed at 473 k) reveals that the amount of some transformed crystalline phases increase with different crystallized particles of sizes appears as shown in Fig. 1(b).
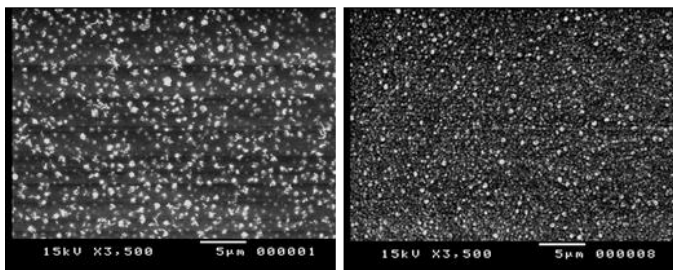

Figure 1. The SEM photograph for $Ge_{20}Se_{70}Zn_{10}$ thin films (a) annealed at 373 K and (b) annealed at 473 K for 1 h.

In order to determine the crystalline phases that appeared in SEM for the annealed $Ge_{20}Se_{70}Zn_{10}$ thin films, the X-ray diffraction of films at different annealing temperature for 1h in nitrogen flow were analyzed. Fig. 2(a–c) shows XRD patterns of as-deposited and annealed samples. The XRD studies show that the as-deposited film is amorphous in nature as shown in Fig. 2(a) but the films annealed show significant improvement in crystallinity and the dominant crystalline phases were GeSe and ZnSe with some traces phase of Se as shown in Fig. 2(b, c). The angle diffraction of the observed X-ray peaks have been compared with the angle diffraction of the Hexagonal structure of ZnSe along with corresponding Miller indices (JCPDS card no. 80-0008) and that one of the standard diffraction lines of the Orthorhombic structure of GeSe (JCPDS card no.74-0372) (Tables I &II). On the other hand the XRD peaks of the film annealed at 473 K, shows decrease in intensity of the diffraction peaks that corresponds to Se phase formed as shown in Fig. 2 (b, c).

The intensity of X-ray diffraction peaks related to Hexagonal structure of ZnSe increase with increasing annealing temperature and the intensity of X-ray diffraction peaks related to Orthorhombic structure of GeSe decrease with increasing annealing temperature. This may be due to increase of Se ions migration with increasing annealing temperature because its high concentration inside thin films and the decreasing intensity of one phase appears as an increasing in another phase vice versa.
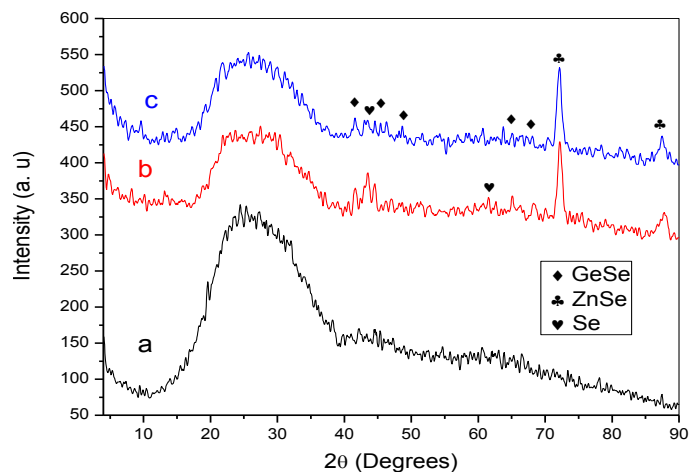

Figure 2. The X-ray patterns of $Ge_{20}Se_{70}Zn_{10}$ thin films, (a) as-deposited (b) annealed at 373 K and (c) annealed at 473K

The average crystal diameter of these phases in spherical approximation have been estimated from the full-width at half maximum (FWHM) of more intensive diffraction peaks according to the Debye-Scherrer model [43].

$$D = \frac{0.94\lambda}{\beta cos\theta} \quad (12)$$

where D is the particle size, λ is the wavelength of used X-ray radiation, β is the angular line width of half maximum intensity and θ is the angle which corresponds to diffraction maximum. We have fitted the diffraction lines of crystalline phases by a Gaussian function to determine the full-width at half maximum as shown in Fig. 3.

The calculated crystal diameter of GeSe and ZnSe phases using equation (12) for annealed thin films are listed in Tables (I & II). They are evident that, the average particle size of the crystallized GeSe phase increases with increasing annealing temperature and the average particle size of the crystallized ZnSe phase decreases with increasing annealing temperature.
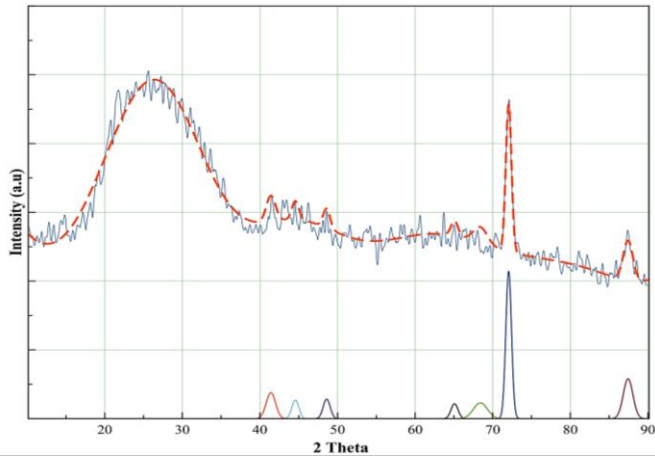

Figure 3. The X-ray pattern of $Ge_{20}Se_{70}Zn_{10}$ thin film thermally annealed at 473 for 1h along with the Gaussian fitting of GeSe and ZnSe crystalline phases. The solid lines represent the experimental data with the Gaussian fitting of GeSe and ZnSe crystalline phases while the dot line represents the fitting by summation of Gaussian curves.

The dislocation density (δ) is deduced as the length of dislocation lines per unit volume of the crystal and is given by

($\delta = 1/D^2$). The strain value (ε) is calculated from the following relation [43],

$$\varepsilon = \left[\frac{\lambda}{D\cos\theta} - \beta\right]\frac{1}{\tan\theta} \tag{13}$$

The results of δ and ε are listed in Tables (I & II). It is observed that the average of strain values and average of dislocation density for GeSe phase decrease whereas particle size increases with increasing the annealing temperature. On the other hand, the average of strain values and average of dislocation density for ZnSe phase increase whereas particle size decreases with increasing the annealing temperature, which indicates the improvement in crystallinity of the present films.

Fig. 4 shows the spectral distribution of transmittance and reflectance for as-deposited and annealed thin films in the wavelength range from 300-2500 nm.

Optical transmission spectra provide useful information about the absorption edge and the optical transmittance. The transmittance spectra obtained from the deposited and annealed films are shown in Fig. 3. The spectra show a high transparency in the visible range above 600 nm. Sharp UV absorption edge at approximately 560 nm is observed for all films. The sharp fall of transmittance at the band edge confirms that the annealed films have a crystalline nature [44]. The high transparency (in the range 600 nm – 2500 nm) presented confirms the good quality of the deposited films and the samples have a smooth surface, which results in less scattering of light and more transmission light [45, 46]. Transmission and reflectance spectra seem to behave in an opposite fashion (see Fig. 4)

TABLE I. STRUCTURE PARAMETERS OF GESE CRYSTALLINE PHASES IN PRESENT THIN FILM AT DIFFERENT ANNEALING TEMPERATURE

$T_{ann.}$	2 theta stand.	2 theta exp.	(hkl)	kind of phase	FWHM	Particle Size (nm)	Average of particle size for GeSe phase (nm)	Average of strain values ($lin^{-2}.m^{-4}$) for GeSe phase	Average of dislocation density $\delta \times 10^{16}$ ($lin./m^2$) for GeSe phase
373 K	41. 868	41.409	(201)	GeSe	0.7034	12.62	13.78	0.00163	0.580
	43.406	43.480	(100)	Se					
	44.416	44.522	(202)	GeSe	0.8839	10.15			
	48.425	48.422	(203)	GeSe	0.5280	17.24			
	62.165	61.540	(200)	Se					
	65.080	65.079	(215)	GeSe	0.7034	14.00			
	68.390	68.235	(310)	GeSe	0.6751	14.86			
473 K	41.868	41.409	(201)	GeSe	0.7034	12.62	15.01	0.00149	0.540
	43.406	42.820	(100)	Se					
	44.416	44.565	(202)	GeSe	0.5280	17.00			
	48.425	48.597	(203)	GeSe	0.5280	17.26			
	62.165	61.780	(200)	Se					
	65.080	65.079	(215)	GeSe	0.5280	18.66			
	68.390	68.410	(310)	GeSe	1.0540	9.52			

$T_{ann.}$	2 theta stand.	2 theta exp.	(hkl)	FWHM	Particle Size (nm)	Average of particle size for ZnSe phase (nm)	Average of strain values (lin^{-2}.m^{-4}) for ZnSe phase	Average of dislocation density $\delta \times 10^{16}$ (lin./m^2) for ZnSe phase
373 K	72.621	72.159	(210)	0.3959	25.95	23.88	0.00061	0.179
	87.341	87.696	(213)	0.5280	21.81			
473 K	72.621	72.057	(210)	0.4301	23.87	19.80	0.00075	0.290
	87.341	87.442	(213)	0.7304	15.73			

Fig. 5 shows the spectral variations of the real refractive index (n) for $Ge_{20}Se_{70}Zn_{10}$ thin films at different annealing temperature, from this figure it is observed that the refractive index can be divided into two regions.

I) A region ($\lambda \leq 665$ nm) in which the refractive index increases with wavelength is said to have anomalous dispersion.

II) A region ($\lambda \geq 665$ nm) in which the refractive index decreases with wavelength is said to have normal dispersion.

It is also observed that the value of refractive index (n) and the height of the peaks decrease with increasing annealing temperature to 423 k, after that increase with increasing annealing temperature. This behavior can be attributed to decrease and increase of tailing in the material [47], as shown in Table III.

Fig. 6 shows the imaginary refractive index (k) for the $Ge_{20}Se_{70}Zn_{10}$ thin films, it is observed that the behavior of the $k(\lambda)$ spectrum is zero in the near infrared (NIR) and infrared (IR) wavelength ranges, whereas in the visible range the imaginary refractive index decreases with increasing wavelength.
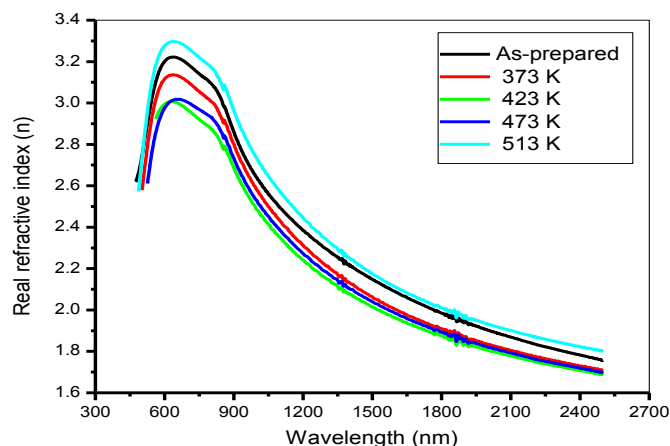

Figure 5. Real refractive index (n) versus wavelength (λ) for the as-deposited and annealed of $Ge_{20}Se_{70}Zn_{10}$ thin films

Figure 6. Imaginary refractive index (k) versus wavelength (λ) for the as-deposited and annealed of $Ge_{20}Se_{70}Zn_{10}$ thin films

Fig. 7 shows typically depandences $(n^2-1)^{-1} = f(E)^2$ for $Ge_{20}Se_{70}Zn_{10}$ thin films. It can observe that the equation (5) could be suitable for the description of the dispersion of refractive index, where the dispersive parameters are shown in Table 3.
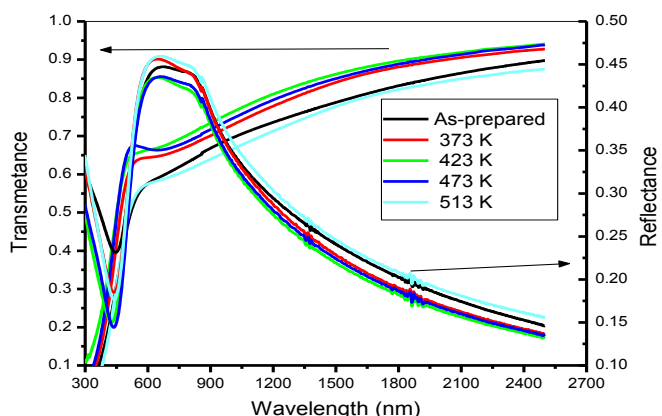

Figure 4. The spectral dependence of transmittance (T) and reflectance (R) for the as-deposited and annealed of $Ge_{20}Se_{70}Zn_{10}$ thin films
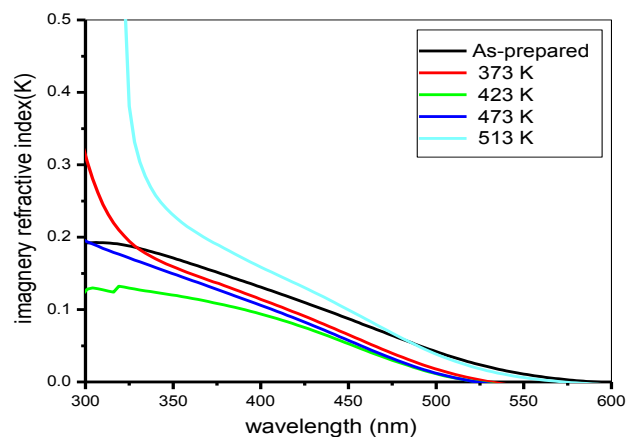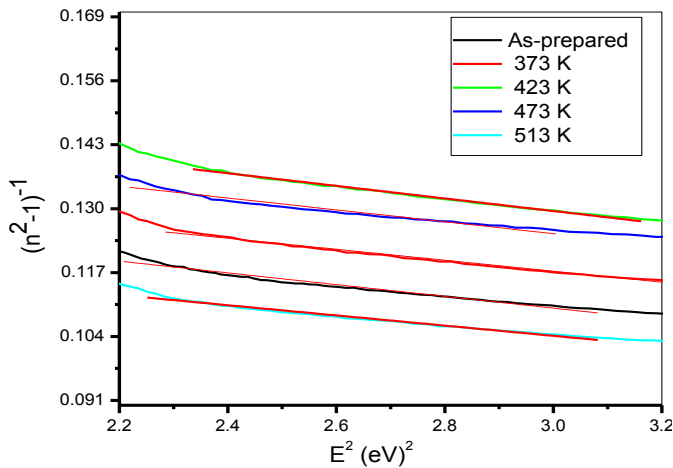
Figure 7. Plots of $(n^2-1)^{-1}$ versus the photon energy $(E)^2$ for the as-deposited and annealed of $Ge_{20}Se_{70}Zn_{10}$ thin films

TABLE III. FITTING PARAMETERS OF REAL REFRACTIVE INDICES, RATIO OF THE CARRIER CONCENTRATION TO THE EFFECTIVE MASS, LATTICE DIELECTRIC CONSTANT, DIRECT ALLOWED OPTICAL ENERGY GAPS AND URBACH ENERGY OF SAMPLES

$T_{ann.}$ For one hour	E_o (eV)	E_d (eV)	n_∞	Nf/m $(m^{-3}kg^{-1})$ $\times10^{58}$	(N/m^*) $\times10^{57}$ m^{-3}/kg	ε_L	E_g (eV)	E_U (eV)
As–deposited	3.515	23.960	2.803	6.711	32.78	4.763	2.78	0.072
373 K	3.497	24.390	2.732	6.255	28.08	4.385	2.84	0.053
423 K	3.465	22.816	2.608	5.514	24.91	4.162	2.89	0.037
473 K	3.328	22.964	2.627	5.175	26.62	4.281	2.85	0.042
513 K	3.193	23.335	2.806	5.548	28.96	4.775	2.65	0.082

Dispersive parameter, Nf/m decreases with increasing annealing temperature except the sample which annealed at 513 K increases with increasing annealing temperature, also n_∞, decreases with increasing annealing temperature up to 473 K followed by a remarkable increases due to further increase of annealing temperature. Table 3 also lists the obtained values of E_o and E_d, for the as-deposited and annealed thin films. It is clear that the values of E_o decrease while the values of E_d increase with increasing the annealing temperatures. These may be due to increase diffusion rate of atoms inside annealed thin films with increasing annealing temperature, leading to generate numbers of sites atoms and increase numbers of scattering center [48, 49]. These results are in good agreement with the previous works [10, 50]. The ratio of the carrier concentration to the effective mass (N/m^*) and lattice dielectric constant (ε_L) for the investigated films also listed in Table (3). It is observed that both (N/m^*) and (ε_L) decrease with increasing annealing temperature.

Fig. 8 shows the relation between $(\alpha.E)^2$ and photon energy (E) to determine the direct optical band gap for as-deposited and annealed thin films. The obtained values of the optical band gap energy (E_g) are listed in Table (3). It is interesting to observe that the value of (E_g) increases from about 2.78 eV (for as-deposited film) to 2.89 eV, after heat treatment at 423 K. The lower value of about 2.78 eV obtained of (E_g) for the non-heated $Ge_{20}Se_{70}Zn_{10}$ sample may be related to the existence of a high density of defects levels within the band gap determined by the amorphous structure of this sample [51]. The increase of (E_g) up to 2.89 eV with increasing annealing temperature may be attributed to the increase in grain size. The further decrease of the optical band gap beginning at an annealing temperature of about 473 K may be due to unsaturated bonds and other structural defects which can introduce localized states in the forbidden band that can be responsible for the narrowing of the band gap [51]. The same behavior was observed for amorphous $As_{45.2}Te_{46.6}In_{8.2}$ and $Ge_{20}Se_{80-X}In_X$ thin films [52, 53],
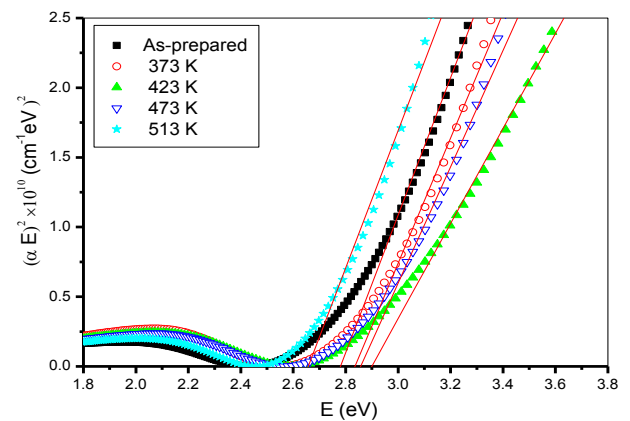

Figure 8. Variation of $(\alpha.E)^2$ as a function of photon energy (E) for the as-deposited and annealed of $Ge_{20}Se_{70}Zn_{10}$ thin films

The values of Urbach energy (E_u) for the $Ge_{20}Se_{70}Zn_{10}$ thin films are shown in Table (3). It can be noted that the Urbach energy decreases from about 0.072 eV (for as- deposited film) to 0.032 eV after heat treatment at 423 K, after that it increases with increasing annealing temperature. The Urbach edge is usually ascribed to localized states at the band edge. It is determined by the degree of disorder and/or structural defects such as broken or dangling bonds, vacancies and non-bridging atoms in the considered sample [54].

VI. CONCLUSION

The present study of $Ge_{20}Se_{70}Zn_{10}$ thin films revealed the following conclusions:

1. Bulk of composition $Ge_{20}Se_{70}Zn_{10}$ was prepared by the melt-quench technique, and thin films were prepared from the bulk of $Ge_{20}Se_{70}Zn_{10}$ by thermal evaporation at vacuum of 10^{-5} Torr.

2. Analytical relations are used to deduce the real and imaginary refractive indices from the measured reflectance and transmittance for as-deposited and different annealing temperature.

3. Dispersion parameters of the imaginary refractive indices have been calculated.

4. The optical absorption measurements for as-deposited and annealed films for $Ge_{20}Se_{70}Zn_{10}$ indicated that the absorption mechanism is due to direct transition.

5. The optical band gap and Urbach energy are sensitive to heat treatment, where the value of (E_g) increases from about 2.78 eV (for as-deposited film) to 2.89 eV after heat treatment at 423 K after that decreases with increasing annealing temperature, whereas (E_u) is an opposite behavior of (E_g).

VII. ACKNOWLEDGEMENTS

REFERENCES

[1] K. Tanaka, and Curr. Opin. Photoinduced processes in chalcogenide glasses, Solid State Mater. Sci. 1 (1996) 567.

[2] Zakery, S. R. Elliott, Optical properties and applications of chalcogenide glasses a review: J. of Non-Cryst. Solids 330 (2003) 1–12.

[3] A. V. Kolobov, Photo-Induced Metastability in Amorphous Semiconductors, Wiley-VCH, 2003.

[4] A. Stronski, O. Paiuk, A. Gudymenko, V. Kladko, P. Oleksenko, N. Vuichyk, M. Vlček, I. Lishchynskyy, E. Lahderanta, A. Lashkul, A. Gubanova, and T. Kryskov, Effect of doping by transitional elements on properties of chalcogenide glasses, Ceram. Int. 41 (2015) 7543–7548.

[5] K. Tanaka, and K. Shimakawa, Amorphous Chalcogenide Semiconductors and Related Materials, Springer, New York, NY, 2011.

[6] O. Mouawad, P. Vitry, C. Strutynski, J. Picot-Clémente, F. Désévédavy, G. Gadret, J.C. Jules, E. Lesniewska, and F. Smektala, Atmospheric aging and surface degradation in As253 fiber in relation with suspended-core profile, Opt. Mater. 44 (2015) 25–32.

[7] M. Nasir, and M. Zulfequar, DC conductivity and dielectric behaviour of glassy $Se_{100-x}Zn_x$ alloy. Open J. Inorg. Non Met. Mater. 2(2), 11–17 (2012).

[8] M.F. Gromboni, T.C. Kastein, R. Matos, and L.H. Mascaro, Characterization and optical properties of ZnSe thin films obtained by electrodeposition technique. ECS Trans. 43(1), (2012), 211–216.

[9] M. A. Abdel-Rahim, M. M. Hafiz, and A. Elwhab. B. Alwany, The effect of composition on structural and optical properties of ZnSe alloys. Opt. Laser Technol. 47, 88–94 (2013).

[10] M.A. Abdel-Rahim, M.M. Hafiz, and A. Elwhab.B. Alwany, Influence of annealing on the structure and optical properties of $Zn_{40}Se_{60}$ thin films. Opt. Laser Technol. 44(4), 1116–1121 (2012).

[11] R. K. Kremer, M. Cardona, R. Lauck, G. Siegle, and A.H. Romero, Vibrational and thermal properties of Zn X (X = Se, Te): density functional theory (LDA and GGA) versus experiment. Phys. Rev. B 85(3), 035208 (2012).

[12] Dohare, N. Mehta, Determination of kinetics parameters of glass transition in glassy Se and glassy Se98M2 alloys using DSC technique. Appl. Phys. A 114(2), (2014), 597–603.

[13] M. Nasir, M.A.M. Khan, M. Husain, and M. Zulfequar, Thermal properties of $Se_{100-x}Zn_x$ glassy system. Mater. Sci. Appl. 2(05), 289 (2011).

[14] Z. U. Borissova, Glassy Semiconductor, (Chapter 1). Plenum Press, New York, 1981.

[15] S.A. Khan, M. Zulfequar, and M. Husain, effect of annealing on crystallization process in amorphous $Ge_5Se_{95-x}Te_x$ thin films, Physica B 324 (2002) 336.

[16] S. Min, H. Yang, and Z. Cheng, the optical and electrical gaps of Ge Se Te, J. Non-Cryst. Solids 52 (1982) 181.

[17] S.A. Fayek, M. El-Oker, and A. S. Hassanien, Optical and electrical properties of $Ge_{10+x}Se_{40}Te_{50-x}$ Mater. Chem. Phys. 70 (2001) 231.

[18] S. Fouad, The glass transition temperature and related parameters in the glassy Ge_xSe_{1-x} system, Physica B 293 (2001) 276-282.

[19] H. El-Zahed, M.A. Khaled, A. El-korashy, S.-M. Yousef, and M. El Oker, Dependence of optical band gap on the compositions of $Se_{(1-x)}Te_x$ thin films, Solid State Commun. 89 (12) (1994) 1013-1016.

[20] H. El-Zahed, A. El-korashy, and M. Dongol, Optical parameter studies of as-deposited and annealed $Se_{1-x}Te_x$ films.Thin Solid Films 259 (1995) 203-211.

[21] A. El-Korashy, H. El-Zahed, H.A. Zayed, and M.A. Kenawy, Effect of composition and structure on electrical conduction of $Se_{(100-x)}Te_{(x)}$ films,Solid State Commun. 95 (5) (1995) 335-339.

[22] A. Bakry, A.S. Soltan, and A. El-Korashy, Radiation effects on the optical properties of $Se_{85-x}Te_{15}Sb_x$ thin films, Rad. Effects defects Solids 160 (7) (2006) 275-284.

[23] H. El-Zahed, A. El-Korashy, and M.A. Abdel-Rahim, Effect of heat treatment on some of the optical parameters of $Cu_9Ge_{11}Te_{80}$ films.Vacuum 68 (2002) 19-27.

[24] H. El-Zahed, and A. El-Korashy, Influence of composition on the electrical and optical properties of $Ge_{20}Bi_xSe_{80-x}$ films. Thin Solid Films 376 (2000) 236-240.

[25] A. El-Korashy, N. El-Kabany, and H. El-Zahed, Optical, electrical and the related parameters of amorphous Ge–Bi–Se thin films.Physica B 365 (2005) 55-64.

[26] R. M. Mehra, G. Kaur, A. Pundir, and P.C. Mathur, Study of Se-Te-Sb system for application to Reversible Optical Data Storage, Jpn. J. Appl. Phys. 32 (1993) 128-129.

[27] Z. Wang, C. Tu, Y. Li, and Q. Chen, The effects of Sn and Bi additions on properties and structure in Ge-Se-Te chalcogenide glass, J. Non-Cryst. Solids 191 (1995) 132-137.

[28] A. S. Soltan, M. Abu E.L-Oyoun, A.A. Abu-Sehly, and A.Y. Abdel-Latief, Thermal annealing dependence of the structural, optical and electrical properties of selenium–tellurium films, Mater. Chem.Phys. 82 (2003) 101-106.

[29] F. Abdel-Wahab, Observation of phase separation in some Se–Te–Sn chalcogenide glasses, Physica B 406 (2011) 1053-1059.

[30] Z. S. E. Mandouh, Transport properties in Se–Te–Ge glasses, J. Appl. Phys. 78 (1995) 7158.

[31] A. P. J. M. Jongenelis, J.H. Coombs, W. van Es-Spiekman, and B.A.J. Jacobs, Laser‐induced crystallization phenomena in GeTe‐based alloys. III. GeTeSe alloys for a CD compatible erasable disk, J. Appl. Phys.79 (1996) 8349.

[32] D.J. Sarrach, J.P. De Neufville, and W.L. Haworth, Studies of amorphous Ge-Se-Te alloys (I): Preparation and calorimetric observations, J. Non-Cryst. Solids 22 (1976) 245-267.

[33] E. M. Vinod, and K. S. Sangunni, The effect of Se doping on spectroscopic and electrical properties of GeTe, Thin Solid Films 550 (2014) 569-574.

[34] M. M. Hafiz, A. H. Moharram, M. A. Abdel-Rahim, and A. A. Abu-Sehly, The effect of annealing on the optical absorption and electrical conduction of amorphous $As_{24.5}Te_{71}Cd_{4.5}$ thin films, Thin Solid Films 292 (1997) 7–13.

[35] M. A. Majeed Kan, M. Zulfequar, and M. Husain, Optical investigation of a-$Se_{100-x}Bi_x$ alloys, Opt. Mater. 22 (2003) 21-29. https://doi.org/10.1016/S0925-3467(02)00234-3

[36] J.Y. Shim, S.W. Park, and H.K. Baik, Silicide formation in cobalt/amorphous silicon, amorphous CoSi and bias-induced CoSi films, Thin Solid Films 292 (1997) 31-39.

[37] S. Hasegawa, S. Yazaki, and T. Shimizu, Effects of annealing on gap states in amorphous Si filmsSolid State Commun 26(1978)407-410.

[38] R. R. Willey, Practical Design and production of Optical Thin Films, Marcel Dekker Inc., New York, 2002.

[39] M. J. Weber, Handbook of Optical Materials, CRC press, Boca Raton, 2003.

[40] S.Y. El-Zaiat, Determination of the complex refractive index of a thick slab material from its spectral reflectance and transmittance at normal incidence. Optik, 124 (2013) 157–161.

[41] Wemple, S.H. and DiDomenico Jr., M. Behavior of the Electronic Dielectric Constant in Covalent and Ionic Materials. Physical Review B, 3(1971), pp. 1338.

[42] F. Urbach, the Long-Wavelength Edge of Photographic Sensitivity and of the Electronic Absorption of Solids, Physical Review, 92(5), (1953), pp. 1324.

[43] S. Venkatachalam, Y. Jeyachandran, P. Sureshkumara, A. Dhayalraj, D. Mangalaraj, K. Narayandass, and S. Velumani, Characterization of vacuum-evaporated ZnSe thin films, Materials Characterization 58 (8-9), (2007), pp. 794–799.

[44] S. Venkatachalam, Yoshinori Kanno, D. Mangalaraj, and Sa. K. Narayandass, Effect of boron ion implantation on the structural, optical and electrical properties of ZnSe thin films, Physica B 390 (2007) 71–78.

[45] Vinoth Kumar Jayaraman, Yasuhiro Matsumoto Kuwabara, Arturo Maldonado Álvarez, and María de la luz Olvera Amador, Importance of substrate rotation speed on the growth of homogeneous ZnO thin films by reactive sputtering, Materials Letters 169(2016), 1-4.

[46] Y.C. Wang, K.J. Shieh, M.S. Shyu, F.L. Shyu, J.S. Shyu, and W.C. Hwang, Diamond-like carbon film overcoats for phase-change optical recording discs, Surface and Coatings Technology 165 (2003), 140–145.

[47] S. Kumar, S. C. Kashiap and K. L. Chopra, Electron transport properties of n-type bismuth modified a-$Ge_{20}Se_{70}$ films. J. Non-Cryst. Solids 85 (1986), pp. 100-104.

[48] M. M. Malik, M. Zulfequar, A.Kumar, and M. Husain. Effect of indium impurities on the electrical properties of amorphous $Ga_{30}Se_{70}$, Journal of Physics: Condensed Matter 4(43) (1992), pp. 8331-8338

[49] V. D. Das, and Mallik, R.C. Study of Scattering of Charge Carriers in Thin Films of $(Bi_{0.25}Sb_{0.75})_2Te_3$ Alloy with 2% Excess Te. Materials Research Bulletin, 37 (2002)1961-1971. 47.

[50] M. A. Abdel-Rahim, M. M. Hafiz, and A. Z. Mahmoud, influence of thermal annealing on structural and optical properties of $Se_{70}Te_{15}Sb_{15}$ Thin Films. Chalcogenide letters 12 (2015) pp. 263-275.

[51] G. G.Rusu, M. Rusu, and M. Girtan, Optical characterization of vacuum evaporated CdZnTe thin films deposited by a multilayer method. Vacuum 81(2007), pp.1476-1479.

[52] A. A. Abu-Sehly, and M.I. Abd-Elrahman, Effect of annealing temperature on the optical and electrical properties of amorphous $As_{45.2}Te_{46.6}In_{8.2}$ thin films. J. Phys. Chem. Sol. 63 (2002) 163-170

[53] S. K. Ishu, and P. B. Tripathia, Barman, Influence of composition on the on the optical band gap in A-$Ge_{20}Se_{80-X}In_X$ thin films. Chalcogenide Letters Vol. 3, No. 12, December (2006), pp. 121-12.

[54] MF. Kotkata, MS. Al-Kotb, and FA. Abdel-Wahab, doping effect of Sm on the energy gap and optical dispersion a-Se .Chalcog. Lett. 2010; 7: 145.